

# Subtype-aware Unsupervised Domain Adaptation for Medical Diagnosis

Xiaofeng Liu<sup>1,2</sup>, Xiongchang Liu<sup>2,3†</sup>, Bo Hu<sup>2,4†</sup>, Wenxuan Ji<sup>5</sup>, Fangxu Xing<sup>1</sup>, Jun Lu<sup>2\*</sup>, Jane You<sup>6</sup>, C.-C. Jay Kuo<sup>7</sup>, Georges El Fakhri<sup>1</sup>, Jonghye Woo<sup>1</sup>

<sup>1</sup>Dept. of Radiology, Massachusetts General Hospital and Harvard Medical School, Boston, MA, USA

<sup>2</sup>Dept. of Neurology, Beth Israel Deaconess Medical Center and Harvard Medical School, Boston, MA, USA

<sup>3</sup>China University of Mining and Technology, China <sup>4</sup>Beijing University of Posts and Telecommunications, China

<sup>5</sup>School of Artificial Intelligence, Nankai University, China

<sup>6</sup>Dept. of Computing, The Hong Kong Polytechnic University, Hong Kong

<sup>7</sup>Dept. of Electrical and Computer Engineering, University of Southern California, Los Angeles, CA, USA

<sup>†</sup>Co-second authors contribute equally \*Corresponding Author

## Abstract

Recent advances in unsupervised domain adaptation (UDA) show that transferable prototypical learning presents a powerful means for class conditional alignment, which encourages the closeness of cross-domain class centroids. However, the cross-domain inner-class compactness and the underlying fine-grained subtype structure remained largely underexplored. In this work, we propose to adaptively carry out the fine-grained subtype-aware alignment by explicitly enforcing the class-wise separation and subtype-wise compactness with intermediate pseudo labels. Our key insight is that the unlabeled subtypes of a class can be divergent to one another with different conditional and label shifts, while inheriting the local proximity within a subtype. The cases of with or without the prior information on subtype numbers are investigated to discover the underlying subtype structure in an online fashion. The proposed subtype-aware dynamic UDA achieves promising results on medical diagnosis tasks.

## Introduction

Unsupervised domain adaptation (UDA) aims to transfer knowledge learned from a label-rich domain to a new unlabeled target domain (Saito et al. 2017a; Liu et al. 2020d; Liu 2020; Zou et al. 2019). The conventional adversarial training and maximum mean discrepancy (MMD) methods propose to align the marginal distribution of sample  $x$  in the feature space, i.e.,  $p(f(x))$ , where  $f$  is a feature extractor. With the Bayes' theorem  $p(f(x)|y) = \frac{p(y|f(x))p(f(x))}{p(y)}$  and assuming no concept and label shifts (i.e.,  $p(y|f(x))$  and  $p(y)$  are the same for two domains), the conditional distribution  $p(f(x)|y)$  can be aligned by aligning  $p(f(x))$ . Nevertheless, the label shift  $p(y)$  is quite common in real-world applications, which indicates the label proportion is different (Zhao et al. 2019).

Recently, transferable prototypical networks (TPN) (Pan et al. 2019) is proposed to encourage the source domain class separation with the cross-entropy (CE) loss, and match the class centroids of source and target samples to achieve class-wise alignment. However, the CE loss on the source domain cannot minimize the inner-class variation (Liu et al. 2016).

Copyright © 2021, Association for the Advancement of Artificial Intelligence (www.aaai.org). All rights reserved.

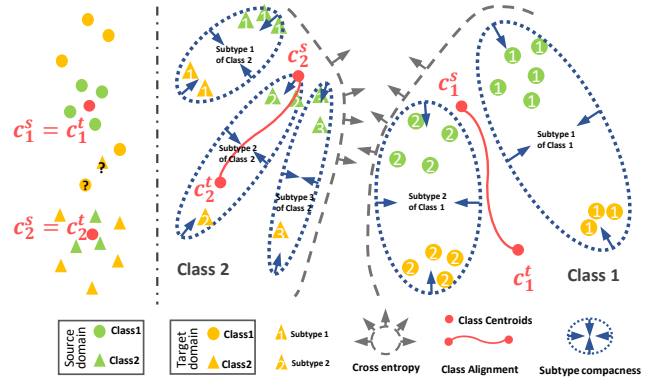


Figure 1: Illustration of the failure case of prototypical UDA (left), and the idea of our subtype-aware UDA (right).

The class-wise separation on the to-be tested target domain cannot be well supported by the centroid closeness objective. As shown in Fig. 1 left, even if the class centroids are well aligned, the sparsely distributed target samples can be easily misclassified.

A possible solution is to simply enforce the cross-domain inner-class feature distribution compactness. However, in many cases, the unlabeled subtypes in a class can be significantly diverse, and form an underlying local distribution. For instance, the different cancer subtypes can have significantly diverse patterns (Yeoh et al. 2002). The shared pattern among the two subtypes may not be exclusive for class-level discrimination. In these applications, it is more reasonable and effective to exploit the subtype-wise patterns. Moreover, unsupervised deep clustering (Caron et al. 2018) empirically assigns  $10\times$  more clusters of the class to contain diverse subtypes. (Chen et al. 2019b) also shows the fine-grained label can be helpful for the coarse classification.

Moreover, the domain shifts can be different w.r.t. subtypes, which results in *subtype conditional shift*. Besides, the incidence of disease subtypes is usually varied across different regions, which results in *subtype label shift*. The proportion difference in the subtype-level can usually be more significant than the class-level (Wu et al. 2019). This moti-

vates us to extend the concept of class conditional and label shifts (Kouw 2018) to the fine-grained subtype-level (i.e.,  $p(f(x)|k)$  and  $p(k)$  vary across domains for the subtype  $k$ ), and a more realistic presumption of UDA can be both the class and subtype conditional and label shifts.

In this paper, we resort to the feature space metric learning with intermediate pseudo labels to adaptively achieve both class-wise separation and cross-domain subtype-wise compactness. We propose an online clustering scheme to explore the underlying subtype structure in an unsupervised fashion. With the prior knowledge of subtype numbers, the concise  $k$ -means clustering can be simply applied by assigning  $k$  to the subtype numbers. However, the subtype can be challenging to define based on different taxonomy. We further expand on our framework to the case of unknown subtype numbers by capturing the underlying subtype structure with an adaptive sub-graph scheme using the reliability-path. With a few meta hyperparameters shared between clusters, the sub-graph scheme can be scalable to many classes and subtypes. To explicitly enforce the subtype-wise distribution compactness, the involved samples of a subtype are expected to be close to their subtype centroid in the feature space.

Our main contribution can be summarized as follow:

- We propose to adaptively explore the subtype-wise conditional and label shifts in the UDA without the subtype labels, and explicitly enforce the subtype-aware compactness.
- We systematically investigate the cases with or without the prior information on subtype numbers. Our reliability-path based sub-graph scheme can effectively explore the underlying subtype local distribution with a few meta hyperparameters in an online fashion.
- We empirically validate its effectiveness on a multi-view congenital heart disease (CHD) diagnosis task with the Depthwise Separable Convolution (DSC)-based efficient multi-view processing network and achieve promising performance.

## Related Work

With the rapid development of machine learning, automated machine analysis and interpretation technology are increasingly used in medicine (Liu et al. 2019a; Han et al. 2020; Liu et al. 2020a). More researchers are turning their attention to the data analysis and identification of medical imaging data (De Fauw et al. 2018). Early attempts extracted the handcrafted features from a cardiovascular image (Maraci et al. 2017) and fed them into the statistical classifier (Liu et al. 2018c; 2017a).

Recently, CNN-based deep learning has gained enormous successes in image analysis tasks (Liu et al. 2019f; 2020f; 2018a; 2019c). Instead of designing features by hand and subsequently feeding the features to a prediction model, deep learning proposes to simultaneously learn relevant features and the prediction model from raw image data in an end-to-end fashion (Che et al. 2019; Liu et al. 2019d; He et al. 2020b; Liu et al. 2020e). Related studies have

shown that by using deep neural networks, machines can effectively identify abnormalities from ultrasonic views (Litjens et al. 2019; Liu et al. 2020c; Che et al. 2019; Liu et al. 2018e).

Compared with over one million images of the ImageNet dataset, the collection of large-scale medical data is challenging for clinical applications (Liu et al. 2020c; 2018d; He et al. 2020a). Recently, UDA has gradually become more popular (Zou et al. 2019; Liu et al. 2020d), which aims to match covariant shift (i.e., only  $p(x)$  shift). Discrepancy-based methods (Long et al. 2015) address the dataset shift by mitigating specific discrepancies defined on different layers of a shared model between domains, e.g., MMD. Recently, adversarial training utilizes a discriminator to classify the domain to encourage domain confusion (Tzeng et al. 2017; Liu et al. 2020b). These methods assume that the label proportion is the same for all of the involved domains (Moreno-Torres et al. 2012). While the conditional shift (Magliacane et al. 2018) (i.e., only  $p(x|y)$  shift) can be more realistic than the covariate shift (Zhao et al. 2019), and the class label shift (i.e., only  $p(y)$  shift) also widely exists in the most of real-world applications (Kouw 2018). Moreover, the subtype-wise conditional and label shifts are also a realistic assumption in many applications, which can be more challenging than the class-wise shifts due to the unavailable of subtypes in both source and target domains.

Recently, pseudo labels of a target domain have been widely used for UDA (Zou et al. 2019; Liu et al. 2020d). The pseudo labels are used to estimate target class centers (Chen et al. 2019a), and the results are enforced to match the source class centers. Contrastive Adaptation Network (Kang et al. 2019) is developed to estimate contrastive domain discrepancy with the target pseudo labels. Considering that the pseudo labels can be noisy, the Gaussian-uniform mixture model is proposed to measure the correctness (Gu, Sun, and Xu 2020). Rather than using the sophisticated noisy model, we propose a noise-robust sub-graph scheme with the simple online semi-hard mining (Liu et al. 2017b; 2019e).

The class-wise conditional alignment (Pan et al. 2019) is proposed by matching the source and target class centers as in (Chen et al. 2019a). Moreover, source centers can be regarded as class protocols for classification. Although the source class-wise separation can be enforced by its CE loss (Liu et al. 2016), the center matching does not encourage the compactness of source and target samples, and can lead to sparse target distribution and considerable inner-class variation.

The center loss (Wen et al. 2016) is proposed to encourage the compact distributed representation feature for face identification. Numerous works (Liu et al. 2017b; 2018b; Xu et al. 2020; Liu et al. 2019e; 2019b) adopt the center loss to metric learning and optimal transport methods. However, the underlying subtype distribution and shifts are largely ignored. Moreover, the online exploring of the subtype proposed in this work is also closely related to the unsupervised deep clustering (Caron et al. 2018). Not limited by using  $k$ -means with the prior knowledge of the subtype numbers, we further propose a scalable sub-graph scheme without the

need for the subtype number. The dynamic memory framework is robust to the pseudo label noise and subtype under-sampling.

## Methodology

We consider the UDA task, where we have a source domain  $p^s(x, y)$  and a target domain  $p^t(x, y)$ , and the learning framework has access to a labeled source set  $\{(x_i^s, y_i^s)\}$  drawn from  $p^s(x, y)$  and an unlabeled target set  $\{(x_i^t)\}$  drawn from  $p^t(x, y)$ . The class label space of  $y_i \in \{1, 2, \dots, N\}$  is shared for both source and target domains. We use  $n$  to index  $N$  classes. For class  $n$ , we assume there are  $K_n$  underlying subtypes indexed with  $k \in \{1, 2, \dots, K_n\}$ . UDA aims to build a good classifier in the target domain  $p^t(x, y)$  with the following theorem:

**Theorem 1** For a hypothesis  $h$  drawn from  $\mathcal{H}$ ,  $\epsilon^t(h) \leq \epsilon^s(h) + \frac{1}{2}d_{\mathcal{H}\Delta\mathcal{H}}\{s, t\} + \min_{h \in \mathcal{H}} [\epsilon^s(h, l_s) + \epsilon^t(h, l_t)]$ .

Here,  $\epsilon^s(h)$  and  $\epsilon^t(h)$  denote the expected loss with hypothesis  $h$  in the source and target domains, respectively. Considering that the disagreement between labeling function  $l_s$  and  $l_t$ , i.e.,  $\min_{h \in \mathcal{H}} [\epsilon^s(h, l_s) + \epsilon^t(h, l_t)]$ , can be small by optimizing  $h$  with the source data (Ben-David et al. 2007), the UDA focuses on minimizing the cross-domain divergence  $d_{\mathcal{H}\Delta\mathcal{H}}\{s, t\}$  in the feature space of  $f(x_i^s)$  and  $f(x_i^t)$ .

Instead of aligning  $p^s(f(x))$  and  $p^t(f(x))$  (Kouw 2018), the prototypical networks propose to match the class centroids (Pan et al. 2019). However, the decision boundary of the low density distributed target sample can be difficult to define, and the inherent subtype structure is underexplored.

On the embedding space, we expect the class separation on the target domain can be achieved when the source domain classes are well-separated, and the class-wise source-target distribution compactness is enforced. Moreover, under the fine-grained subtype local structure and their conditional and label shifts, the subtype-wise tight clustering can be a good alternative to achieve class-wise alignment and compactness. Accordingly, we have the following proposition:

**Proposition 1.** The class-wise compactness can be a special case of subtype-wise compactness by assigning the subtype number of this class to 1.

Targeting the conditional and label shifts in both class-level ( $p^s(f(x)|y) \neq p^t(f(x)|y), p^s(y) \neq p^t(y)$ ) and subtype-level ( $p^s(f(x)|k) \neq p^t(f(x)|k), p^s(k) \neq p^t(k)$ ), we propose a novel subtype-aware alignment framework based on an adaptive clustering scheme as in Fig. 1.

### Class-wise source separation and matching

Forcing the separation of classes on the source domain,  $p^s(x, y)$ , can be achieved by the conventional CE loss (Liu et al. 2016). With the extracted features, we carry out the classification via a remold of the distance to each class cluster center (Chen et al. 2019a; Pan et al. 2019).

For the labeled source data  $\{(x_i^s, y_i^s)\}$ , we represent the feature distribution of class  $n$  with a class centroid  $c_n^s =$

$\frac{1}{M_c^s} \sum_{i=1}^{M_c^s} f(x_i^s)$ , where  $M_c^s$  is the involved source sample number. For an input source sample  $x_i^s$ , we can directly produce a probability histogram with the softmax normalized distance between  $x_i^s$  and the centroids  $c_n^s$ . Specifically, the probability of  $x_i^s$  belonging to class  $n$  can be formulated as

$$p(y_i^s = n | x_i^s) = \frac{e^{-\|f(x_i^s) - c_n^s\|_2^2}}{\sum_{n=1}^N e^{-\|f(x_i^s) - c_n^s\|_2^2}}. \quad (1)$$

With the one-hot encoding of true class  $n$ , we define the class-wise cross-entropy loss for the source domain samples as  $\mathcal{L}_{CE}^{class} = -\log p(y_i^s = n | x_i^s)$ .

Following the self-labeling scheme (Zou et al. 2019; Pan et al. 2019), each target sample  $x_i^t$  is assigned with a pseudo class label  $\hat{y}_i^t$  to its nearest source centroids, i.e.,  $\hat{y}_i^t = n$  if  $\min_n \|f(x_i^t) - c_n^s\|_2^2$ . With the pseudo class label  $\hat{y}_i^t$ , we calculate the target domain class-level centroids  $c_n^t = \frac{1}{M_c^t} \sum_{i=1}^{M_c^t} f(x_i^t)$ , where  $M_c^t$  is the involved target sample number. We expect the close proximity of  $c_n^s$  and  $c_n^t$  with  $\mathcal{L}^{class} = \frac{1}{N} \sum_{n=1}^N \|c_n^s - c_n^t\|_2^2$ , which is not sensitive to label shift, since it only chooses the representative centroids of source and target distribution<sup>1</sup>. However, neither  $\mathcal{L}_{CE}^{class}$  nor  $\mathcal{L}^{class}$  considers the inner-class compactness (Wen et al. 2016) and the fine-grained subtype structure.

### Subtype-aware alignment with $K_n$ prior

If the subtype numbers  $K_n$  of class  $n$  is known (e.g., 4 subtypes in CHD disease dataset), we can achieve feature space class-independent clustering with the concise  $K$ -means, by defining  $K$  to  $K_n$ .

We denote  $K_n$  clustered subtypes with  $k \in \{1, 2, \dots, K_n\}$ , and calculate the source and target subtype centroids  $\mu_k^s$  and  $\mu_k^t$ , respectively. However,  $K$ -means does not assign the specific class label to each cluster. To correlate the source and target clusters, we rank the distance of  $K_n^2$  subtype centroid pairs and link the smallest rank first.

Because of the imbalance distribution of subtypes and possible label shift, we assign the subtype centroids of both the source and target samples with  $\mu_k^{st} = \frac{\mu_k^s + \mu_k^t}{2}$  instead of averaging all of the source and target samples in subtype  $k$ . Therefore, each subtype in both source and target domains contributes equally to  $\mu_k^{st}$ . Then, we enforce all of the samples in subtype  $k$  to be close to the subtype centroid  $\mu_k^{st}$ . For the sake of simplicity, we omit the class notation. The subtype compactness objective  $\mathcal{L}_k^{sub}$  can be

$$\frac{1}{M_k^s} \sum_{i=1}^{M_k^s} \|f(x_i^s) - \mu_k^{st}\|_2^2 + \frac{1}{M_k^t} \sum_{i=1}^{M_k^t} \|f(x_i^t) - \mu_k^{st}\|_2^2, \quad (2)$$

where  $M_k^s$  and  $M_k^t$  are the numbers of source and target samples in subtype  $k$ , respectively, to balance the subtype

<sup>1</sup>The source & target center  $c_n^{st} = \frac{\sum_{i=1}^{M_c^s + M_c^t} f(x_i^{st})}{M_c^s + M_c^t}$  used in (Pan et al. 2019), and its objective of close proximity of  $c_n^s \leftrightarrow c_n^{st}$ , or  $c_n^t \leftrightarrow c_n^{st}$  are not robust to label shift. Note that  $c_n^{st}$  will change if we simply double the involved source/target samples.

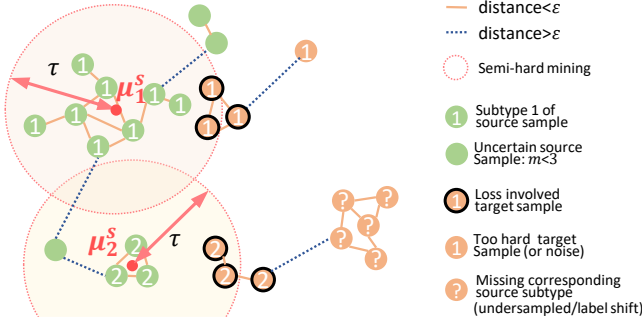


Figure 2: Illustration of the reliability-path based sub-graph construction and alignment with  $m = 3$ . ? will be assigned to subtype 2, which will then be rejected by  $\tau$ .

label shift.  $\mathcal{L}_k^{sub}$  is traversed for  $N$  classes and their  $K_n$  subtypes to calculate the sum of normalized subtype compactness loss  $\mathcal{L}^{sub} = \frac{1}{N} \sum^N (\frac{1}{K_n} \sum^{K_n} \mathcal{L}_k^{sub})$ . Note that an image that does not belong to class  $n$  does not belong to any of its  $K_n$  subtypes. The class-wise matching and subtype-wise compactness objectives can be aggregated as a hierarchical alignment loss  $\frac{1}{N} \sum^N (\alpha \mathcal{L}^{class} + \beta \frac{1}{K_n} \sum^{K_n} \mathcal{L}_k^{sub})$ , where  $\alpha$  and  $\beta$  are the balancing parameters. In the feature space, the learned representations are expected to form  $K_n$  compact clusters for class  $n$ , while each cluster does not need to be far away from one another.

### Reliability-path based sub-graph construction

Defining or estimating  $K_n$  can be difficult in many applications. Setting  $K_n$  of all classes as  $N$  hyper-parameters requires costly trials considering the diverse value range of different classes. Note that with a deterministic encoder  $f$ , the distribution protocol can be similar among different subtypes and classes (Fahad et al. 2014).

Therefore, we propose to construct the sub-graph with the reliability-path to achieve the online source domain subtype clustering. We assume that similar samples are likely to be distributed closely in the feature space with a deterministic encoder  $f$  and form a high-density region (Carlucci et al. 2019). Given  $M^s$  samples from the class  $n$  in the source domain, there are  $(M^s)^2$  possible edges in a graph. To explore the local structure of the feature space, the two nodes  $\{f(x_i^s), f(x_j^s)\}$  are connected by the reliability-path, if  $\|f(x_i^s) - f(x_j^s)\|_2^2 \leq \epsilon$ . The directly or indirectly linked nodes are combined to form a sub-graph.

To further eliminate the effect of noise and undersampled subtypes on a batch, we only select the sub-graphs with more than  $m$  nodes as the valid subtype clusters.

After exploring the  $K_n$  subtypes in the source domain and calculating their centroids  $\mu_k^s$ , we assign each target sample with the pseudo label of class  $n$  to the subtype with the most similar centroid (i.e.,  $\min_k \|f(x_i^t) - \mu_k^s\|_2^2$ ).

Considering the relatively low confidence or reliability of pseudo target labels (Zou et al. 2019; Gu, Sun, and Xu 2020), we adopt a simple online semi-hard mining scheme to select the target sample in a subtype. The cross-domain

margin  $\tau$  is used to define a circle at the center of  $\mu_k^s$ . For the target sample with the initial pseudo subtype label  $k$ , we choose these samples to distribute within the circle. We note that some target samples may be densely distributed around the circle boundary, and it is not reasonable to cut them apart simply. Therefore, we also resort to the reliability-path to involve the closely distributed neighboring target samples. The sub-graph construction can be robust to missing subtypes in the source or target domain caused by undersampling, since  $m$  filters the unreliable source cluster out, and the self-labeling with semi-hard mining of  $f(x_i^t)$  rejects the additional subtypes in the sampled target domain. The operation is illustrated in Fig. 2.

With the reliability-path connected  $M_k^s$  source samples and the refined  $M_k^t$  target samples in subtype  $k$ , we calculate  $\mu_k^{st} = \frac{\mu_k^s + \mu_k^t}{2}$ , and enforce the subtype-wise compactness with  $\mathcal{L}_k^{sub}$  as in Eq. (2).

The online sub-graph construction and alignment have three hyperparameters, including  $\epsilon$ ,  $\tau$ , and  $m$  that are shared for all classes and their subtypes, which can be regarded as the meta-knowledge across clusters. Moreover, we can simplify  $\epsilon$  to be the constant 1, and change it to any other positive value results only in the matrices being multiplied by corresponding factors (Liu et al. 2017b). The range of  $m$  can also be narrow and similar among different subtypes/classes.

### Optimization and implementation

The modern neural networks usually extract a high-dimensional vector, e.g., 4,096 or 2,048-dimensional features, as their representation, thereby resulting in high memory and time complexity in subsequent clustering. To remedy this, deep clustering (Caron et al. 2018) proposes to perform dimension reduction via PCA on the features across the entire dataset. PCA, however, is not applicable anymore in our online SubUDA. The features of different samples have varying timestamps, thus resulting in incompatible statistics among samples. It is also computationally demanding to carry out PCA in each iteration. Accordingly, a non-linear head layer of fc-bn-relu-dropout-fc-relu is adopted in order to reduce high dimensional features into 256 dimensions. As well, it is jointly optimized during online SubUDA iterations. The head layer is eliminated for downstream tasks, e.g., calculating the L2 distance between features.

In order to circumvent the training from collapsing into a few subtype clusters, (Caron et al. 2018) makes uniform sampling before each epoch, which, however, is difficult in our online UDA setting, due to the missing of subtype and target class labels. We propose a concise approach for SubUDA via re-weighting the loss with  $\omega_k \propto \frac{1}{\sqrt{M_k^s + M_k^t}}$ , according to the number of samples in the  $k_{th}$  subtype.

Therefore, samples in smaller clusters contribute more to back-propagation, which thereby pushes the decision boundary away to incorporate more potential samples. The optimization objective can be summarized as

$$\mathcal{L} = \mathcal{L}_{CE}^{class} + \frac{1}{N} \sum^N (\alpha \mathcal{L}^{class} + \beta \frac{\omega_k}{K_n} \sum^{K_n} \mathcal{L}_k^{sub}). \quad (3)$$

For the classification in testing, we utilize the centroids of training features as prototypical (Pan et al. 2019).

## Experiments

We carry out experiments on medical subtype data to evaluate the effectiveness of our approach. We implement our methods using PyTorch and set  $\alpha = 1$ ,  $\lambda = 0.5$ , and  $\beta = 0.5$  consistently.

Congenital heart disease (CHD) is one of the most common birth defects and the leading cause of death in neonates. Its clinical diagnosis is usually based on selected 2D key-frames from five-view echocardiograms. We collect five-view echocardiograms of 1,608 labeled source subjects (normal/patient) from Beijing Children’s Hospital (BCH) and 800 unlabeled target subjects from Harvard Medical School (HMS). Each patient has the echocardiogram records from 1 to 5 views that can be sufficient for diagnosis.

To quantify the effect of subtype structure, the four subtypes of CHD (i.e., ASD, VSD, PDA, and TOF) were confirmed by either at least two senior ultrasound doctors or intraoperative final diagnosis. We note that the fine-grained subtype label is not used in training, since the large-scale labeling can be costly in clinical practice, while the normal/patient label can be relatively easy to acquire by the primary doctors. Of note, this work focuses on exploring the subtype-aware alignment for the conventional class-wise discriminative model.

We note that the diseased area and pattern in different subtypes are different; therefore different subtypes can be more easily detected from different views. Considering the large inner-class variation of patient class, it is reasonable to enforce the subtype-wise compactness. In Fig. 4 left, we can see that the source CHD samples of a subtype also tend to be distributed closely, demonstrating the underlying inner-subtype similarity. With our subtype-wise compactness objective, both the source and target samples are grouped into the high-density region w.r.t. subtypes.

### Standard collection of cardiac ultrasound images

- BCH source domain.** A total of 1,608 children (823 healthy controls, 209 VSD, 276 ASD, 124 TOF, and 176 PDA) were collected. The patient was placed in the supine position and the chest was exposed for the echocardiogram. We used PHILIPS iE 33 (Philips Electronics Nederland B.V.) for the acquisition. The transducer frequency was ranging from 3 to 8 MHz. According to the heart segmental approach, the heart position, atrial position, and ventricular position were determined, and the connection relationship between the atria, ventricle, and aorta was analyzed. The atrial septum and ventricular septum were investigated whether there were defects, and cavity or pulmonary venous return was noted. Five standard 2D views, the parasternal long-axis view (PSLAX) of the left ventricle, the parasternal short-axis view (PSSAX) of the aorta, the apical four chambers view (A4C), the subxiphoid long-axis view (SXLAX) of two atriums, and the suprasternal long-axis view (SSLAX) of aortic arch were collected.

- HMS target domain.** In total of 800 children (300 healthy controls, 150 VSD, 150 ASD, 100 TOF, and 100

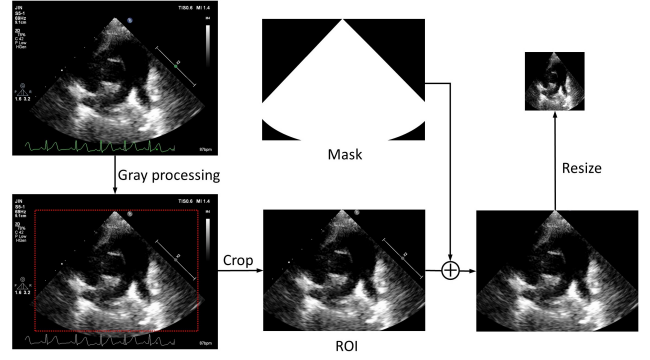


Figure 3: Data pre-processing flowchart.

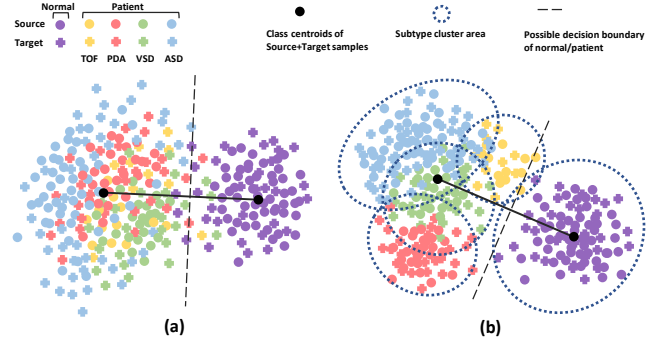


Figure 4: T-SNE visualization of the sampled CHD features with (a) TPN (Pan et al. 2019) and (b) our SubUDA. We normalized the distance between class centroids to demonstrate the class separation and inner-class/subtype compactness.

PDA) were collected. Each patient was placed in the supine position and the chest was exposed for the echocardiogram. We used PHILIPS EPIQ 7C (Philips Electronics Nederland B.V.) for the acquisition. The transducer frequency was ranging from 3 to 8 MHz. According to the heart segmental approach, the heart position, atrial position, and ventricular position were determined, and the connection relationship between the atria, ventricle, and aorta was analyzed. The atrial septum and ventricular septum were investigated whether there were defects, and cavity or pulmonary venous return was noted. Five standard 2D views, the parasternal long-axis view (PSLAX) of the left ventricle, the parasternal short-axis view (PSSAX) of the aorta, the apical four chambers view (A4C), the subxiphoid long-axis view (SXLAX) of two atriums, and the suprasternal long-axis view (SSLAX) of aortic arch were collected.

In summary, the possible discrepancies between these two medical centers can be imaging devices (PHILIPS iE 33 vs. EPIQ 7C), patient populations, and the echocardiogram imaging experience of clinical doctors.

The key-frame was manually selected by the experienced doctor. Specifically, we labeled the isovolumic relaxation phase as a key-frame when the ventricles finished contracting and started to relax, the defects of VSD and ASD both could be shown clearly at that time.



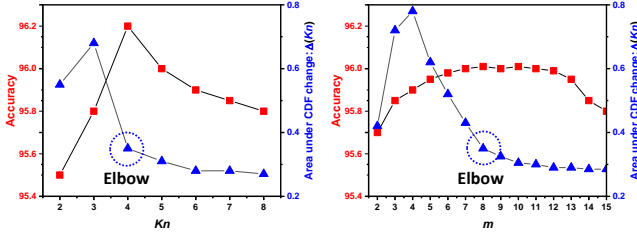


Figure 5: The sensitive analysis of  $K_n$  (right) and  $m$  of patient class in CHD dataset.

We selected 20% patients from HMS to construct our fixed testing set in a patient-independent manner. Note that the videos or keyframes used in training will not be incorporated in testing.

### Pre-processing

We first processed each frame to a single-channel grayscale image, and the region of interest (ROI) was cropped to remove the irrelevant parts. Since the collected ultrasonic image was a circular sector, and some labels could not be removed by rectangular cropping, a mask was designed to cover these factors. To align with the input of conventional CNNs, the masked ROI was resized to  $128 \times 128$ . We used the same pre-processing for the image of each view and concatenated these five images following fixed order: PSLAX of the left ventricle, PSSAX of the aorta, A4C, SXLAX of two atriums, and SSLAX of the aortic arch. Noticing that each view only had one image in our 2D echocardiogram dataset.

### Backbone network structure for CHD task

The limited training dataset can be difficult to support the tuning of the network with a large number of parameters, usually resulting in overfitting. To alleviate this problem in our congenital cardiovascular disease diagnosis task, the Depthwise Separable Convolution (DSC) (Howard et al. 2017) is adopted to largely reduce the network parameters. In DSC, the convolution process is broken down into two operations: depth-wise convolutions and point-wise convolutions. In depth-wise operation, convolution is applied to a single channel at a time unlike standard CNN’s in which it is done for all the  $N$  channels. The widely used AlexNet (Simonyan and Zisserman 2014) has 60 million to-be-learned parameters, while the DSC (with width multiplier 0.50) (Howard et al. 2017) can achieve comparable performance in the ImageNet object classification dataset using only 1.32 million parameters. Noting that since the DSC is originally designed for RGB data, which is different from our input, we inherit the idea of the DSC to construct our multi-channel CNN.

The diagnosis of congenital cardiovascular disease is more challenging than a common object recognition task, because of its multi-view data structure as well as the relatively limited and unbalanced training sample. The decision is based on five views, which can incorporate more complementary information than a single view-based diagnosis. However, this also introduces the challenge of information

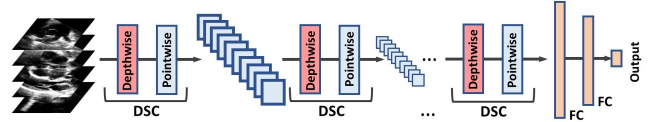


Figure 6: Illustration of the multichannel convolutional neural networks for key frame-based multi-view diagnosis.

Table 1: Multi-channel DSC network architecture. dw denotes the depth-wise convolution with size  $H \times W$ , and keep the same for  $N$  channels. pw denotes the point-wise convolution with size  $1 \times 1 \times N$ . The first layer uses the conventional convolution with stride size 2 (Howard et al. 2017).

| Input Size                | Type / Stride | Filter Shape                              |
|---------------------------|---------------|---|
| $128 \times 128 \times 5$ | Conv / s2     | 32 kernels of $3 \times 3 \times 5$       |
| $64 \times 64 \times 32$  | Conv dw / s1  | 32 kernels of $3 \times 3$ dw             |
| $64 \times 64 \times 32$  | Conv pw / s1  | 64 kernels of $1 \times 1 \times 32$ pw   |
| $64 \times 64 \times 64$  | Conv dw / s2  | 64 kernels of $3 \times 3$ dw             |
| $32 \times 32 \times 64$  | Conv pw / s1  | 128 kernels of $1 \times 1 \times 64$ pw  |
| $32 \times 32 \times 128$ | Conv dw / s2  | 128 kernels of $3 \times 3$ dw            |
| $16 \times 16 \times 128$ | Conv pw / s1  | 128 kernels of $1 \times 1 \times 128$ pw |
| $16 \times 16 \times 128$ | Conv dw / s2  | 128 kernels of $3 \times 3$ dw            |
| $8 \times 8 \times 128$   | Conv pw / s1  | 128 kernels of $1 \times 1 \times 128$ pw |
| $8 \times 8 \times 128$   | Flatten       | N/A                                       |
| 8192                      | FC1           | 1024                                      |
| 1024                      | FC2           | 128                                       |
| 128                       | Classifier    | Softmax                                   |

fusion. We propose to concatenate the five views sequentially, and produce a matrix with size  $128 \times 128 \times 5$ . A five-channel CNN, as shown in Figure 6, is developed to take the concatenated matrix as input. Each DSC block incorporates a depthwise convolution and a pointwise convolution. After a few DSC layers, the feature maps are flattened as the feature vector that is processed by two fully connected layers with sizes 1024 and 128, respectively. The detailed network structure is given in Table 1.

We note that the multi-branch framework can be an alternative to the multi-channel network (Lee, Lee, and Kim 2016). However, the multi-channel scheme can adaptively learn the information fusion in each layer, instead of the simple concatenation in a fully connected layer (Lee, Lee, and Kim 2016). The different views of echocardiograms also share some similarities. Therefore, the filters learned in a view may potentially be helpful in the other view. Moreover, the multi-channel model with a single-branch can have significantly fewer parameters than the multi-branch counterpart. The fewer parameter is important for the limited training data. Besides, the memory cost of the multi-channel module is much fewer than the multi-branch module. We note that the multi-channel model is not applicable for heterogeneous inputs (e.g., image and EEG data), since they require different network structure for different inputs. With sufficiently large training datasets, the performance of multi-branch and multi-channel are usually similar for homogeneous input (Lee, Lee, and Kim 2016).

For the binary classification (negative or positive), we use

| Method                             | Accuracy (%) $\uparrow$ | AUC $\uparrow$    |
|------------------------------------|-------------------------|-------------------|
| Source only                        | 76.4 $\pm$ 0.12         | 0.721 $\pm$ 0.005 |
| MCD (Saito et al. 2017b)           | 88.6 $\pm$ 0.15         | 0.856 $\pm$ 0.003 |
| GTA (Sankaranarayanan et al. 2018) | 90.9 $\pm$ 0.17         | 0.873 $\pm$ 0.005 |
| CRST (Zou et al. 2019)             | 93.2 $\pm$ 0.09         | 0.882 $\pm$ 0.006 |
| TPN (Pan et al. 2019)              | 93.4 $\pm$ 0.14         | 0.885 $\pm$ 0.004 |
| SubUDA ( $K_n = 4$ )               | 96.2 $\pm$ 0.13         | 0.910 $\pm$ 0.003 |
| SubUDA ( $K_n = 1$ )               | 94.7 $\pm$ 0.11         | 0.902 $\pm$ 0.004 |
| SubUDA- $\mu_k^{st}$ ( $K_n = 4$ ) | 95.4 $\pm$ 0.10         | 0.903 $\pm$ 0.005 |
| SubUDA- $\omega_k$ ( $K_n = 4$ )   | 96.0 $\pm$ 0.13         | 0.908 $\pm$ 0.004 |
| SubUDA-DR ( $K_n = 4$ )            | 96.2 $\pm$ 0.11         | 0.911 $\pm$ 0.002 |
| SubUDA-SG ( $m = 8$ )              | 96.0 $\pm$ 0.12         | 0.907 $\pm$ 0.004 |
| SubUDA-SG- $\tau$ ( $m = 8$ )      | 95.5 $\pm$ 0.14         | 0.902 $\pm$ 0.003 |

Table 2: Experimental results for CHD.  $\uparrow$  larger is better.

the sigmoid function as the output unit and optimize the network with binary cross-entropy loss.

## Evaluations

For comparison, we re-implement the current state-of-the-art methods with the same backbone and experiment setting. We choose the batch size to 64. The results are shown in Table. 2. Considering the imbalance of health and patient proportion in the testing set, we also provide the area under the receiver operating characteristic curve (AUC) metric in addition to the accuracy metric.

MCD (Saito et al. 2017b) and GTA (Sankaranarayanan et al. 2018) are the typical adversarial training framework to align the marginal distribution  $p(x)$  in feature level or image-level, respectively. (Zou et al. 2019) utilizes the self-training to alternatively update the pseudo label of target samples and the network parameters. We note that the compared methods (Saito et al. 2017b; Sankaranarayanan et al. 2018; Zou et al. 2019; Wu, Inkpen, and El-Roby 2020) use the fully-connected classifier after the encoder. The TPN (Pan et al. 2019) uses class centroids as classifiers. It proposes to align class centroids of source and target sample to achieve the conditional alignment w.r.t.  $p(x|y)$ . The proposed SubUDA outperforms the previous state-of-the-art methods w.r.t. both the accuracy and AUC by a large margin, by introducing the subtype-aware constraint. The results indicate that the online subtype compactness can effectively help the classification in the target domain.

The domain adaptation theory suggests proxy  $\mathcal{A}$ -distance (Ben-David et al. 2007) as a measure of cross-domain discrepancy (Saito, Ushiku, and Harada 2017). In Fig. 7, we compare our SubUDA with the other state-of-the-art methods, and the smaller discrepancy has been observed by using the explicit compactness objective in our SubUDA.

For the ablation study, with  $K_n = 1$ , the subtype-wise alignment will degenerate to the class-wise compactness. Besides, we use the suffix -DR,  $-\omega_k$ , and  $-\tau$  to denote the subUDA without dimension reduction head, subtype balance weight, and semi-hard target mining, respectively. Be-

sides, the suffix  $-\mu_k^{st}$  denotes using  $\mu_k^{st} = \frac{\sum_{i=1}^{M_k^s + M_k^t} f(x_i^{st})}{M_k^s + M_k^t}$  as the subtype centroid, which is not robust to the subtype label shift. SubUDA-DR takes  $4\times$  clustering time, but the improvement is marginal. Therefore, we recommend using

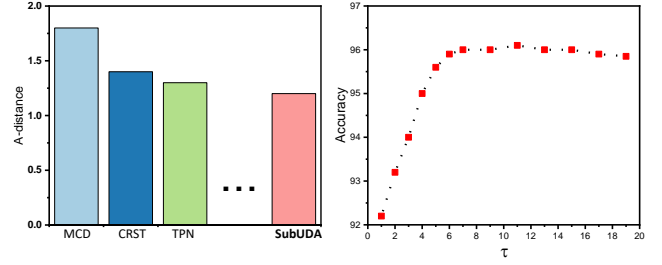


Figure 7: Comparison with the other STOs w.r.t.  $\mathcal{A}$ -distance (left), and the sensitive analysis of  $\tau$  (right).

the dimension reduction head.

SubUDA-SG in Tab. 2 uses the reliability-path based online sub-graph to replace  $k$ -means. With appropriate  $m = 8$ , the adaptively learned clustering can achieve comparable performance to the  $k$ -means with  $K_n = 4$ . In Fig. 7 right, we can see that the semi-hard mining in SubUDA-SG is not sensitive to the  $\tau$  for a large range, since the network can flexibly learn to adjust the ratio of  $\epsilon$  and  $\tau$  in mapping space (Liu et al. 2017b). We note that too strict semi-hard mining (i.e., too small  $\tau$ ) can degenerate our SubUDA to conventional class centroids matching, since no target samples will be selected to form a subtype cluster.

In Fig. 5, we provide a sensitive analysis of hyperparameter  $K_n$  and  $m$  for two kinds of online clustering schemes. Consensus clustering is a way of assessing the clustering stability (Monti et al. 2003), and the optimal clustering is usually achieved in the elbow position of the area under CDF changes, where the CDF is for the consensus matrices<sup>2</sup>. We can see that the peak of accuracy usually coincides with the best clustering consensus metric, which indicates the good subtype clustering can boost the SubUDA performance. The choice of  $K_n = 4$  also matches our prior knowledge of CHD patient subtypes.

Since we have clear four subtypes in this task, using the concise  $k$ -means can be a straightforward solution. However, Fig. 5 right shows that the accuracy curve can be robust for a relatively large range of  $m$ , which is promising for the hyperparameter tuning of the case without the prior information of subtype numbers.

## Conclusion

In this paper, we have presented a more realistic assumption in domain adaptation that the subtype-wise conditional and label shifts widely exist, and can be adaptively aligned without the subtype label. We systematically investigate the flexible solution for the case of w/o the prior knowledge of subtype numbers. Rather than the concise  $k$ -means, we further generate our framework with an online sub-graph scheme using the reliability-path, which can be scalable to many classes and subtypes with a few meta hyperparameters. The effectiveness of explicitly enforcing the subtype-aware compactness has been successfully demonstrated in CHD transfer tasks.

<sup>2</sup>[https://github.com/ZigaSajovic/Consensus\\_Clustering](https://github.com/ZigaSajovic/Consensus_Clustering)

## Acknowledgements

We would like to thank anonymous reviewers greatly for their valuable comments.

## References

- Ben-David, S.; Blitzer, J.; Crammer, K.; and Pereira, F. 2007. Analysis of representations for domain adaptation. In *NIPS*.
- Carlucci, F. M.; D’Innocente, A.; Bucci, S.; Caputo, B.; and Tommasi, T. 2019. Domain generalization by solving jigsaw puzzles. In *CVPR*.
- Caron, M.; Bojanowski, P.; Joulin, A.; and Douze, M. 2018. Deep clustering for unsupervised learning of visual features. In *ECCV*, 132–149.
- Che, T.; Liu, X.; Li, S.; Ge, Y.; Zhang, R.; Xiong, C.; and Bengio, Y. 2019. Deep verifier networks: Verification of deep discriminative models with deep generative models. In *ArXiv*.
- Chen, C.; Xie, W.; Huang, W.; Rong, Y.; Ding, X.; Huang, Y.; Xu, T.; and Huang, J. 2019a. Progressive feature alignment for unsupervised domain adaptation. In *CVPR*.
- Chen, Z.; Ding, R.; Chin, T.-W.; and Marculescu, D. 2019b. Understanding the impact of label granularity on cnn-based image classification. *arXiv:1901.07012*.
- De Fauw, J.; Ledsam, J. R.; Romera-Paredes, B.; Nikolov, S.; Tomasev, N.; Blackwell, S.; Askham, H.; Glorot, X.; O’Donoghue, B.; Visentin, D.; et al. 2018. Clinically applicable deep learning for diagnosis and referral in retinal disease. *Nature medicine* 24(9):1342–1350.
- Fahad, A.; Alshatri, N.; Tari, Z.; Alamri, A.; Khalil, I.; Zomaya, A. Y.; Foufou, S.; and Bouras, A. 2014. A survey of clustering algorithms for big data: Taxonomy and empirical analysis. *IEEE transactions on emerging topics in computing* 2(3):267–279.
- Gu, X.; Sun, J.; and Xu, Z. 2020. Spherical space domain adaptation with robust pseudo-label loss. In *Proceedings of the IEEE/CVF Conference on Computer Vision and Pattern Recognition*, 9101–9110.
- Han, Y.; Liu, X.; Sheng, Z.; Ren, Y.; Han, X.; You, J.; Liu, R.; and Luo, Z. 2020. Wasserstein loss-based deep object detection. In *Proceedings of the IEEE/CVF Conference on Computer Vision and Pattern Recognition (CVPR) Workshops*.
- He, G.; Liu, X.; Fan, F.; and You, J. 2020a. Classification-aware semi-supervised domain adaptation. In *Proceedings of the IEEE/CVF Conference on Computer Vision and Pattern Recognition (CVPR) Workshops*.
- He, G.; Liu, X.; Fan, F.; and You, J. 2020b. Image2audio: Facilitating semi-supervised audio emotion recognition with facial expression image. In *Proceedings of the IEEE/CVF Conference on Computer Vision and Pattern Recognition (CVPR) Workshops*.
- Howard, A. G.; Zhu, M.; Chen, B.; Kalenichenko, D.; Wang, W.; Weyand, T.; Andreetto, M.; and Adam, H. 2017. Mobilenets: Efficient convolutional neural networks for mobile vision applications. *arXiv preprint arXiv:1704.04861*.
- Kang, G.; Jiang, L.; Yang, Y.; and Hauptmann, A. G. 2019. Contrastive adaptation network for unsupervised domain adaptation. In *CVPR*.
- Kouw, W. M. 2018. An introduction to domain adaptation and transfer learning. *arXiv:1812.11806*.
- Lee, D.; Lee, J.; and Kim, K.-E. 2016. Multi-view automatic lip-reading using neural network. In *Asian conference on computer vision*, 290–302. Springer.
- Litjens, G.; Ciompi, F.; Wolterink, J. M.; de Vos, B. D.; Leiner, T.; Teuwen, J.; and Išgum, I. 2019. State-of-the-art deep learning in cardiovascular image analysis. *JACC: Cardiovascular Imaging* 12(8):1549–1565.
- Liu, W.; Wen, Y.; Yu, Z.; and Yang, M. 2016. Large-margin softmax loss for convolutional neural networks. In *ICML*.
- Liu, X.; Kong, L.; Diao, Z.; and Jia, P. 2017a. Line-scan system for continuous hand authentication. *Optical Engineering* 56(3):033106.
- Liu, X.; Vijaya Kumar, B.; You, J.; and Jia, P. 2017b. Adaptive deep metric learning for identity-aware facial expression recognition. In *CVPR*.
- Liu, X.; B.V.K, K.; Yang, C.; Tang, Q.; and You, J. 2018a. Dependency-aware attention control for unconstrained face recognition with image sets. In *European Conference on Computer Vision*.
- Liu, X.; Ge, Y.; Yang, C.; and Jia, P. 2018b. Adaptive metric learning with deep neural networks for video-based facial expression recognition. *Journal of Electronic Imaging* 27(1):013022.
- Liu, X.; Li, Z.; Kong, L.; Diao, Z.; Yan, J.; Zou, Y.; Yang, C.; Jia, P.; and You, J. 2018c. A joint optimization framework of low-dimensional projection and collaborative representation for discriminative classification. In *2018 24th International Conference on Pattern Recognition (ICPR)*, 1493–1498. IEEE.
- Liu, X.; Zou, Y.; Kong, L.; Diao, Z.; Yan, J.; Wang, J.; Li, S.; Jia, P.; and You, J. 2018d. Data augmentation via latent space interpolation for image classification. In *2018 24th International Conference on Pattern Recognition (ICPR)*, 728–733. IEEE.
- Liu, X.; Zou, Y.; Song, Y.; Yang, C.; You, J.; and K Vijaya Kumar, B. 2018e. Ordinal regression with neuron stick-breaking for medical diagnosis. In *Proceedings of the European Conference on Computer Vision (ECCV)*, 0–0.
- Liu, S.; Wang, Y.; Yang, X.; Lei, B.; Liu, L.; Li, S. X.; Ni, D.; and Wang, T. 2019a. Deep learning in medical ultrasound analysis: a review. *Engineering*.
- Liu, X.; Guo, Z.; Jia, J.; and Kumar, B. 2019b. Dependency-aware attention control for imageset-based face recognition. In *IEEE Transactions on Information Forensics and Security*.
- Liu, X.; Guo, Z.; Li, S.; You, J.; and B.V.K, K. 2019c. Dependency-aware attention control for unconstrained face recognition with image sets. In *ICCV*.
- Liu, X.; Han, X.; Qiao, Y.; Ge, Y.; Li, S.; and Lu, J. 2019d. Unimodal-uniform constrained wasserstein training



- for medical diagnosis. In *Proceedings of the IEEE International Conference on Computer Vision Workshops*, 0–0.
- Liu, X.; Kumar, B. V.; Jia, P.; and You, J. 2019e. Hard negative generation for identity-disentangled facial expression recognition. *Pattern Recognition* 88:1–12.
- Liu, X.; Zou, Y.; Che, T.; Ding, P.; Jia, P.; You, J.; and Kumar, B. V. 2019f. Conservative wasserstein training for pose estimation. In *Proceedings of the IEEE/CVF International Conference on Computer Vision (ICCV)*.
- Liu, X.; Xing, F.; Yang, C.; Kuo, C.-J.; El Fakhri, G.; and Woo, J. 2020a. Symmetric-constrained irregular structure inpainting for brain mri registration with tumor pathology. In *MICCAI BrainLes*.
- Liu, X.; Che, T.; Lu, Y.; and Yang, C. 2020b. Auto3d: Novel view synthesis through unsupervisedly learned variational viewpoint and global 3d representation. *ECCV*.
- Liu, X.; Fan, F.; Kong, L.; Xie, W.; Lu, J.; and You, J. 2020c. Unimodal regularized neuron stick-breaking for ordinal classification. *Neurocomputing*.
- Liu, X.; Hu, B.; Liu, X.; Lu, J.; You, J.; and Kong, L. 2020d. Energy-constrained self-training for unsupervised domain adaptation. *ICPR*.
- Liu, X.; Ji, W.; You, J.; Fakhri, G. E.; and Woo, J. 2020e. Severity-aware semantic segmentation with reinforced wasserstein training. In *Proceedings of the IEEE/CVF Conference on Computer Vision and Pattern Recognition*, 12566–12575.
- Liu, X.; Jin, L.; Han, X.; Lu, J.; You, J.; and Kong, L. 2020f. Identity-aware facial expression recognition in compressed video. *ICPR*.
- Liu, X. 2020. Disentanglement for discriminative visual recognition. *arXiv preprint arXiv:2006.07810*.
- Long, M.; Cao, Y.; Wang, J.; and Jordan, M. I. 2015. Learning transferable features with deep adaptation networks. *ICML*.
- Magliacane, S.; van Ommen, T.; Claassen, T.; Bongers, S.; Versteeg, P.; and Mooij, J. M. 2018. Domain adaptation by using causal inference to predict invariant conditional distributions. In *NIPS*.
- Maraci, M. A.; Bridge, C. P.; Napolitano, R.; Papa-georgiou, A.; and Noble, J. A. 2017. A framework for analysis of linear ultrasound videos to detect fetal presentation and heartbeat. *Medical image analysis* 37:22–36.
- Monti, S.; Tamayo, P.; Mesirov, J.; and Golub, T. 2003. Consensus clustering: a resampling-based method for class discovery and visualization of gene expression microarray data. *Machine learning* 52(1-2):91–118.
- Moreno-Torres, J. G.; Raeder, T.; Alaiz-Rodríguez, R.; Chawla, N. V.; and Herrera, F. 2012. A unifying view on dataset shift in classification. *Pattern Recognition* 45(1):521–530.
- Pan, Y.; Yao, T.; Li, Y.; Wang, Y.; Ngo, C.-W.; and Mei, T. 2019. Transferrable prototypical networks for unsupervised domain adaptation. In *CVPR*.
- Saito, K.; Ushiku, Y.; Harada, T.; and Saenko, K. 2017a. Adversarial dropout regularization. *arXiv preprint arXiv:1711.01575*.
- Saito, K.; Watanabe, K.; Ushiku, Y.; and Harada, T. 2017b. Maximum classifier discrepancy for unsupervised domain adaptation.
- Saito, K.; Ushiku, Y.; and Harada, T. 2017. Asymmetric tri-training for unsupervised domain adaptation. In *ICML*.
- Sankaranarayanan, S.; Balaji, Y.; Castillo, C. D.; and Chellappa, R. 2018. Generate to adapt: Aligning domains using generative adversarial networks. In *CVPR*.
- Simonyan, K., and Zisserman, A. 2014. Very deep convolutional networks for large-scale image recognition. *arXiv preprint arXiv:1409.1556*.
- Tzeng, E.; Hoffman, J.; Saenko, K.; and Darrell, T. 2017. Adversarial discriminative domain adaptation. In *CVPR*.
- Wen, Y.; Zhang, K.; Li, Z.; and Qiao, Y. 2016. A discriminative feature learning approach for deep face recognition. In *European Conference on Computer Vision*, 499–515. Springer.
- Wu, Y.; Winston, E.; Kaushik, D.; and Lipton, Z. 2019. Domain adaptation with asymmetrically-relaxed distribution alignment. *arXiv:1903.01689*.
- Wu, Y.; Inkpen, D.; and El-Roby, A. 2020. Dual mixup regularized learning for adversarial domain adaptation. *ECCV*.
- Xu, R.; Liu, P.; Wang, L.; Chen, C.; and Wang, J. 2020. Reliable weighted optimal transport for unsupervised domain adaptation. In *CVPR*.
- Yeoh, E.-J.; Ross, M. E.; Shurtleff, S. A.; Williams, W. K.; Patel, D.; Mahfouz, R.; Behm, F. G.; Raimondi, S. C.; Relling, M. V.; Patel, A.; et al. 2002. Classification, subtype discovery, and prediction of outcome in pediatric acute lymphoblastic leukemia by gene expression profiling. *Cancer cell* 1(2):133–143.
- Zhao, H.; Combes, R. T. d.; Zhang, K.; and Gordon, G. J. 2019. On learning invariant representation for domain adaptation. *arXiv:1901.09453*.
- Zou, Y.; Yu, Z.; Liu, X.; Kumar, B.; and Wang, J. 2019. Confidence regularized self-training. *ICCV*.